論 文

大 韓 造 船 學 會 論 文 集
第 32 卷 第 2 號 1995年 5月
Transactions of the Society of
Naval Architecture of Korea
Vol. 32, No. 2, May, 1995

Computation of Turbulent Appendage-Flat Plate Juncture Flow

by

Sun-Young Kim* and Kazu-hiro Mori**

부가물-평판 접합부 주위의 난류유동 계산

김선영, Kazu-hiro Mori

Abstract

The turbulent flow around the strut mounted on the plate is studied numerically. The main objective of this paper is to validate the numerical scheme by the comparison of the computed results with the measured one, especially, to investigate the applicability of the Baldwin-Lomax(B-L) model to the juncture flow.

Computations are made by solving Reynolds-averaged Navier-Stokes equation with MAC method. The computed results are compared with experimental data of Dickinson[3], collected in the wind tunnel at DTRC. Comparisons show good agreements generally except at the region of wake and very near the juncture. Reynolds stress model seems to be required to improve the accuracy of computation at the region. It can be concluded that B-L model is practically applicable to the juncture flow in spite of the many simplification of the turbulence modelling in B-L model.

요 약

평판 위에 놓여진 스트럿(strut) 주위의 난류유동을 MAC 방법에 의하여 수치계산하였다. 난류모델은 Baldwin-Lomax 모델이며 평판과 스트럿의 접합부 부근에서의 처리를 위하여 Buleev의 m2ixing length를 도입하였다. 계산결과의 검증을 위하여 DTRC의 풍동 실험 결과와 비교하였다. 실험에서 나타난 horseshoe vortex가 계산에서도 재현되는 등 전반적으로 계산결과와 실험결과 간에 좋은 일치를 볼 수 있었다. 그러나 접합부에서 극히 가까운 부근과 스트럿의 후류에서는 불일치를 보여 이 곳에서의 난류모델의 개선이 필요한 것으로 보여졌다. 결론적으로 평판과 스트

Manuscript received : May 13, 1994, Received maneuscript received : December 7, 1994

* Member, Korea Research Institute of Ship and Ocean Engineering

** Hiroshima University

럿의 접합부 부근의 유동을 계산함에 있어서 Baldwin-Lomax 모델은 도입된 많은 단순화를 위한 가정에도 불구하고 실용적으로 유용한 결과를 주는 것으로 보여진다.

1. Introduction

Recently, interests in the juncture flows have been increased in ship hydrodynamics because of the demand for high speed ships. Since high speed ships require both high powering system and safe controllability, they often have more and larger appendages than conventional ships. It follows that the appendage resistance takes large portion of the total resistance for high speed ships. To estimate the appendage resistance accurately, it requires the knowledge of the structure of juncture flow.

The juncture flow formed in the juncture between the appendage and the hull is characterized by the horseshoe vortices which are generated near the leading edge of the appendage. The flow is completely three-dimensional and it becomes more complicated as the horseshoe vortices interact with the boundary layer flow developed on the appendage.

Many experimental studies have been carried out so far to investigate the detailed mechanism of the juncture flow with a simple strut-plate juncture model[4-10]. Although they are of great help to understand the flow, some uncertainties are still remained due to the lack of the resolution of the experimental data. Numerical computation seems to be required to get more information. Furthermore it is of practical importance to develop a numerical code for the design of appendage configuration with smaller drag and good efficiency.

To simulate the juncture flow by solving Navier-Stokes equations, we meet a number of difficulties. Among these are, overcoming an enormous computational time needed to resolve all of the scales involved and finding a turbulence model that provides a sufficiently accurate representation of the various three-dimensional shear layers with separation and reattachment. Today's rapid advance in computer enables us to carry out computation with a grid of high resolution to a extent. On the other hand, any existing turbulence model have still limits in describing the complicated flow near the juncture and in the separated wake region because all the turbulence model up to now are developed based on the experimental data with a simple geometry and flow.

Recently, computational works on the juncture flow have been made by Sung and Yang[10], Chen and Patel[11], and Burke[12] with a Baldwin-Lomax model(B-L model), a two-layer model and a simple mixing length model as a turbulence model respectively. They compared computed results with DTRC experimental data[3] and the comparisons show general good agreements. Their results encourage us to extend our laminar code to turbulent code by introducing B-L model. Although B-L model is a simple eddy-viscosity algebraic model, it would be worth while to be evaluated for juncture flow. This is because even other higher order model is not valid any more very close to the wall. It seems that B-L model can describe rather accurately with a high clustered grid near the wall.

The main objective of this paper is to validate the numerical scheme, especially, to investigate the applicability of the B-L model. Computations are made by solving Reynolds-averaged Navier-Stokes equation with MAC method which was developed for the computation of the laminar juncture

flow[1,2]. Comparison of the computed results are made with experimental data of Dickinson[3] collected in the wind tunnel at David Taylor Research Center. Generally they show good agreements in spite of the many simplification of the turbulence modelling in B-L model. Through the comparison, the practical applicability and the limit of the B-L model to the juncture flow are discussed.

2. Computational Method

2.1 Governing Equation

The governing equations for the incompressible turbulent flow are given by the Reynolds averaged Navier-Stokes and continuity equations. With Boussinesq's eddy viscosity hypothesis, they can be written in the nondimensionalized form as follows;

$$\begin{aligned}
&u_t+uu_x+vu_y+wu_z=-p_x+\frac{1}{R_n}\nabla^2u\\
&+\nu_t(2u_x)_x+\nu_t(u_y+v_x)_y+\nu_t(u_z+w_x)_z\\
&v_t+uv_x+vv_y+wv_z=-p_y+\frac{1}{R_n}\nabla^2v\\
&+\nu_t(u_y+v_x)_x+\nu_t(2v_y)_y+\nu_t(v_z+w_y)_z \quad (1)\\
&w_t+uw_x+vw_y+ww_z=-p_z+\frac{1}{R_n}\nabla^2w\\
&+\nu_t(u_z+w_x)_x+\nu_t(v_z+w_y)_y+\nu_t(2w_z)_z
\end{aligned}$$

$$u_x+v_y+w_z=0\ , \qquad (2)$$

where subscripts represent partial differentiations with respect to the referred variables and (u, v, w) and p are the velocity components in (x, y, z)-direction of the cartesian coordinates and the static pressure respectively. ν_t represents the eddy viscosity. All the variables are nondimensionalized by the chord length of the strut L, the uniform flow velocity U_o, and the density of water ρ. R_n is the Reynolds number based on U_o and L.

A body-fitted coordinate system is adopted and transformation is given by

$$\xi=\xi(x,y,z),\ \eta=\eta(x,y,z),\ \zeta=\zeta(x,y,z)\ . \qquad (3)$$

With these relations, the following transformed governing equations are obtained.

$$\begin{aligned}
&u_t+Uu_\xi+Vu_\eta+Wu_\zeta=\frac{1}{R_n}\nabla^2u\\
&\quad-(\xi_xp_\xi+\eta_xp_\eta+\zeta_xp_\zeta)+R_x\\
&v_t+Uv_\xi+Vv_\eta+Wv_\zeta=\frac{1}{R_n}\nabla^2v\\
&\quad-(\xi_yp_\xi+\eta_yp_\eta+\zeta_yp_\zeta)+R_y \qquad (4)\\
&w_t+Uw_\xi+Vw_\eta+Ww_\zeta=\frac{1}{R_n}\nabla^2w\\
&\quad-(\xi_zp_\xi+\eta_zp_\eta+\zeta_zp_\zeta)+R_z
\end{aligned}$$

$$\begin{aligned}
&\xi_xu_\xi+\eta_xu_\eta+\zeta_xu_\zeta+\xi_yv_\xi+\eta_yv_\eta\\
&+\zeta_yv_\zeta+\xi_zw_\xi+\eta_zw_\eta+\zeta_zw_\zeta=0\ , \qquad (5)
\end{aligned}$$

where R_x, R_y and R_z represent the Reynolds stress terms transformed from the last three terms of RHS of Eq.(1) and U, V and W are the contravariant velocity components defined as

$$\begin{aligned}
U&=\xi_xu+\xi_yv+\xi_zw\\
V&=\eta_xu+\eta_yv+\eta_zw \qquad (6)\\
W&=\zeta_xu+\zeta_yv+\zeta_zw\ .
\end{aligned}$$

Laplacian ∇^2 can be expressed in the body fitted coordinates in the following form;

$$\begin{aligned}
\nabla^2q=&\ \hat{a}q_{\xi\xi}+\hat{b}q_{\eta\eta}+\hat{c}q_{\zeta\zeta}\\
&+2\hat{d}q_{\xi\eta}+2\hat{e}q_{\eta\zeta}+2\hat{f}q_{\zeta\xi} \qquad (7)\\
&+\hat{g}q_\xi+\hat{h}q_\eta+\hat{i}q_\zeta
\end{aligned}$$

where $\hat{a}$, $\hat{b}$ and so on are defined as

$$\begin{aligned}
&\hat{a}=\nabla\xi\cdot\nabla\xi,\ \hat{b}=\nabla\eta\cdot\nabla\eta,\\
&\hat{c}=\nabla\zeta\cdot\nabla\zeta,\ \hat{d}=\nabla\xi\cdot\nabla\eta,\\
&\hat{e}=\nabla\eta\cdot\nabla\zeta,\ \hat{f}=\nabla\zeta\cdot\nabla\xi, \qquad (8)\\
&\hat{g}=\nabla^2\xi,\ \hat{h}=\nabla^2\eta,\ \hat{i}=\nabla^2\zeta\ .
\end{aligned}$$

2.2 Numerical Scheme and Boundary Condition

The computations are made by MAC method

where Poisson equation for the pressure is derived by taking a divergence of the momentum equation and satisfying the continuity equation. The Poisson equation for the pressure is solved iteratively by using the relaxation method and the velocities are updated from the momentum equation. The finite difference equations are derived on a regular grid system. So all the variables are defined on the grid nodes. For the spatial differencing scheme, 2nd order central difference is used while the upwind scheme for the convective term. The Euler explicit scheme is used for the time marching procedure. The computation starts from the still state and the flow is accelerated up to a given constant velocity for the numerical stability.

A C-type grid is adopted for the computation. The coordinate system and grid topology are shown in Fig.1. In the physical domain, a space-fixed cartesian coordinate system is used whose origin is located at the center of the strut on the plate and x-, y- and z- axes are in the uniform flow, lateral and vertical direction respectively. In the transformed body-fitted coordinate system, $\xi-$ and $\eta-$axes are the girthwise of the strut and the normal to the surface of strut and $\zeta-$axis coincides with z-axis. Therefore the surface of the strut lies in the $\eta-$constant plane and the plate lies in the $\zeta-$constant plane. On the strut and the plate, no-slip condition is used for the velocity and Neumann condition is obtained from the momentum equation for the pressure. Outer boundaries are taken on the plate including the inflow and the lateral boundaries where a turbulent boundary layer profile with constant pressure is prescribed while the v-component of velocity is obtained from the momentum equation. The inflow profile is determined by specifying the position of the leading edge of the plate. The height of the strut is assumed to be infinite and the zero gradient conditions are used for all variables.

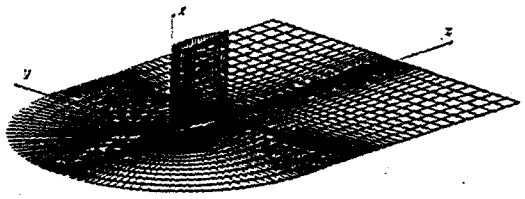

Fig. 1 Grid and coordinate system for DTRC model

On the downstream boundary, the velocities are linearly extrapolated in the streamwise direction by assuming the diffusion in the streamwise direction is negligible but zero gradient condition is used for the pressure.

2.3 Turbulence Model

The turbulence model for the flow around the juncture is complicated and not well developed yet. In this study, the turbulence transport is described by using an algebraic eddy-viscosity model proposed by Baldwin & Lomax[13] which has been used widely in computational fluid dynamics for its simplicity. Modified length scale[14] is incorporated into a Baldwin-Lomax model to treat the corner flow where the turbulence is influenced by both plate and strut.

The procedure of applying Baldwin-Lomax model for the corner flow is as follows. As sketched in Fig.2, in each (J-K) sectional plane, the computational domain is a corner formed by two walls. The local coordinates (n_y, n_z) will be used for the discussion which has an origin on the corner. The eddy viscosity ν_t is computed in the inner and outer regions separately. In the inner region, the eddy viscosity is given by the Prandtl-van Driest formulation

$$(\nu_t)_{inner} = (\kappa\, Dl)^2\, |\omega| \,, \qquad (9)$$

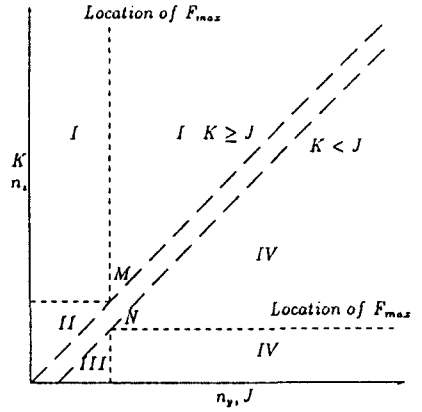

Fig. 2 Definition for the coner flow

where $\varkappa = 0.4$ is von Karman's constant and $|\omega|$ is the magnitude of the vorticity. The definition of l is critical for the evaluation of the eddy viscosity. Buleev's mixing length[15] for the open corner formed by the normal intersection of two planes is used for the present study. It is represented by following formula.

$$l = \frac{2 n_y n_z}{n_y + n_z + (n_y^2 + n_z^2)^{1/2}} \quad . \tag{10}$$

The van Driest damping factor D is given by

$$D = 1 - \exp(- l^+ / 26) \tag{11}$$

and

$$l^+ = \frac{u_\tau \, l}{\nu} = \frac{l}{\nu} \sqrt{\frac{\tau_w}{\rho}} \tag{12}$$

where τ_w is the wall shear stress.

In the outer region,

$$(\nu_t)_{outer} = k \, C_{cp} \, F_{wake} \, F_{kleb} \tag{13}$$

where

$$F_{wake} = \text{smaller of} \begin{cases} l_{max} F_{max} \\ 0.25 \, l_{max} U_{DIF}^2 / F_{max} \end{cases} \tag{14}$$

The quantity U_{DIF} is the difference between the maximum and the minimum resultant velocity in the profile.

$$U_{DIF} = (\sqrt{u^2 + v^2 + w^2})_{MAX} - (\sqrt{u^2 + v^2 + w^2})_{MIN} \tag{15}$$

In the above formulation, k=0.0168 is the Clauser's constant and the quantity F_{max} is the maximum value of $F(l) = l|\omega| D$, and l_{max} is the value of l at which F_{max} occurs. The Klebanoff intermittency factor F_{kleb} is given by

$$F_{kleb} = [\, 1 + 5.5 (\frac{C_{kleb} \, l}{l_{max}})^6 \,]^{-1} \quad . \tag{16}$$

In the outer formulation, the constants C_{cp} and C_{kleb} depend on the condition of flow[16]. In this study, however, $C_{cp} = 1.6$ and $C_{kleb} = 0.3$ are used, which were recommended originally by Baldwin and Lomax[13]. There are some ambiguity in finding F_{max} because several peaks are present in the profile of F for the complex flow as pointed out by Visbal and Knight[16]. The outermost peak is chosen as F_{max} among several peaks to avoid the abrupt change of the computed length scale in the streamwise direction. However, if the chosen peak is smaller than the 20% of the maximum value of F in the profile, it is discarded to avoid finding the peak in the outside of the boundary layer.

The plane is divided into four regions I, II, III and IV as shown in Fig. 2. In regions I and II, D is evaluated at the wall $n_y = 0$ for region I and in regions III and IV, it is evaluated at the wall $n_z = 0$. The search for F_{max} proceeds outward from the wall either from $n_y = 0$ for the region I or from $n_z = 0$ for the region IV. The values of F_{max} in the regions II and III are constant, equal to the value of F_{max} at M and N respectively. Similar treatment is also applied to the wake region by assuming the slip wall on the

center wake plane.

3. Validation of Computation

3.1 Review of Experiments at DTRC

The computed results will be compared with the experimental Data of Dickinson[3] that were measured to serve as a test case for the numerical modelling of the juncture flow. The experiments were carried out in the wind tunnel at DTRC of which the test section is 0.61m × 1.22m and 4.57m long. The strut was mounted on the top of the tunnel that was used as the flat plate of the appendage juncture. Corner fillets were added to the juncture between the top and side walls of the tunnel to reduce the corner secondary flows. The strut was assumed to be semi-infinite, spanning the height of the wind tunnel corresponding to 4 times of the chord length of the strut. The strut has the section which consists of a 3:2 elliptical nose and NACA0020 tail joined at the location of maximum thickness. The resulting strut has a chord of 25.9cm and a thickness of 6.1cm, giving a 10% of blockage ratio. A 3:2 elliptical leading edge was chosen to strengthen the cross-stream flow. The strut was fitted with 0.33mm trip wires at 5% chord.

The experiments were made at the Reynolds number of 5×10^5, based on the free stream velocity and the chord length of the strut. The experimental data include the oil film visualizations, static pressure distribution on the flat plate and the hot-film anemometer measurements of mean and fluctuating velocity components on the seven planes shown in Fig.3. The inflow at the upstream plane located at x=-0.75 was thought of as a two-dimensional fully developed turbulent boundary layer. In this upstream plane, the 99% boundary-layer thickness is about 2.5 inch. with a momentum thickness Reynolds number of approximately 15,000.

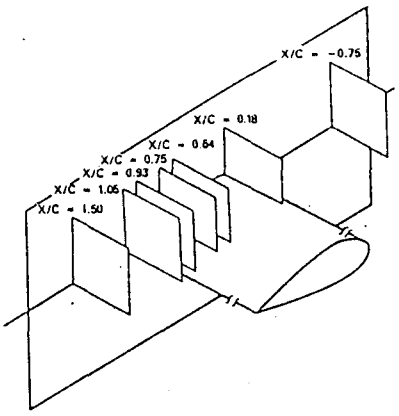

Fig. 3 Measurements planes in DTRC data

3.2 Computational Condition

The flow is assumed to be fully turbulent so that the transition on the strut is not considered. The computation has been made at the Reynolds number of 5×10^5. Based on the measured data on the upstream plane x=-0.75, the 1/6.75-th boundary layer with a boundary layer thickness 0.245 is specified at the upstream and side boundaries. In other words, the 1/6.75-th boundary layer is assumed to be developed from the leading edge of the plate at x=-17. With this inflow condition, the boundary layer thickness at the leading edge but without the strut becomes 0.254. Good agreements between the computed and the measured velocity profile at the upstream plane (x=-0.75), as shown in Fig.14(a), confirms the reasonable inflow boundary condition.

The flow is assumed to be symmetry so that only half of the flow region is computed. In the computation with half C-grid, the number of grid points is 81×41×35 and the minimum spacing and the time step are 0.0002 and 0.0001 respectively. Fig.1 shows the grid and coordinates system used for the present computation.

The computing domain is as follows:

$-2.0 \le x \le 4.0, 0.0 \le y \le 2.2, 0.0 \le z \le 1.0$

The flow is accelerated until t=0.5 and the computation is done up to t=5.0. Fig.4 shows the convergence history of the forces acting on the strut. Here, C_{dp} and C_{df} are pressure drag and frictional drag coefficients nondimensionalized by $0.5\rho L^2U^2$ respectively..

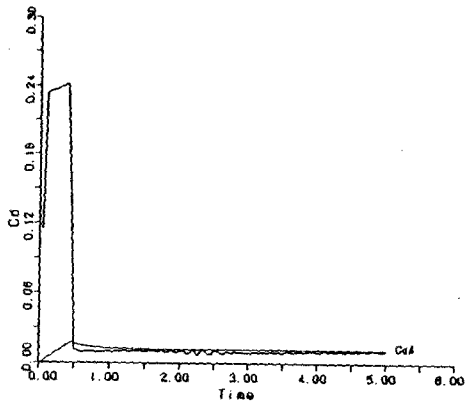

Fig. 4 Convergence history of the forces acting on the strut

3.3 Results and Discussion

The computed particle paths on the upstream symmetry plane, shown in Fig.5, show the existence of the primary and secondary vortex clearly. Both are located closer to the plate. The secondary vortex is extremely small in size and confined to the corner so that it seems difficult to verify its presence in experiments. The position of the core of the computed primary vortex is (-0.07, 0.0065).

In Fig.6, the simulated limiting streamlines on the plate are compared with the oil-film flow visualization results. Both show the separation line wrapping the strut and "V" shaped line behind the trailing edge. The separation point in front of the strut lies -0.17 in computation and it is a little farther from the leading edge than that in experiment. However the breadth of the "V" shaped line

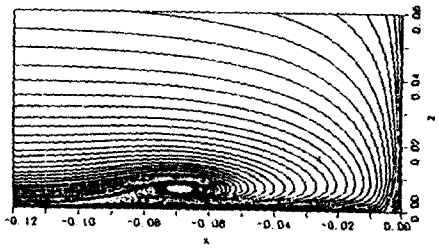

Fig. 5 Particle path on the plane of symmetry upstream

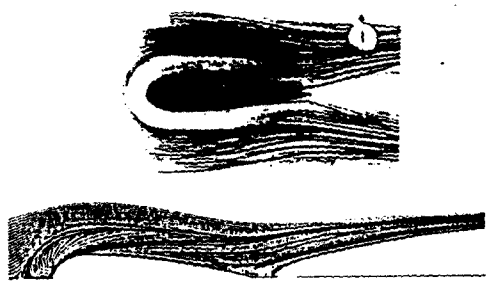

Fig. 6 Limiting streamlines on plate and oil-film visualization results

agrees with the visualized results quite well. The attachment line can be also found near the strut. The primary vortex travels down between the primary separation line and the attachment line while secondary vortex between the attachment line and strut. The separation appears near the trailing edge in the computed flow although no separation was observed in the experiments[3]. This may be due to the insufficient grid resolution as Sung[10] showed that the size of trailing edge flow separation can be much reduced by using finer grids. The more detailed description on the flow structure of the juncture flow including separation can be found in the references[17,18].

When the vortex is close to the body, the surface pressure is dropped due to the acceleration of the flow by the vortex there.

Thus we can see the footprint of the horseshoe vortex from the pressure distribution on the plate shown in Fig.7. There are kinks in the contours around the leading edge which reflect the horseshoe vortex over the plate. We can see two horseshoe vortices travelling downstream around the strut; larger kinks are due to the primary vortex and the the smaller ones closer to the body are due to the secondary horseshoe vortex.

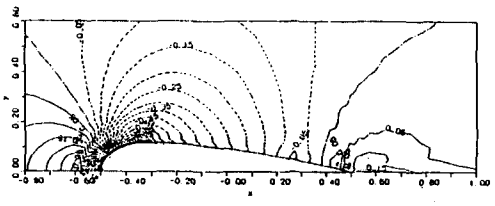

Fig. 7 Pressure contours on the plate

Fig.8 shows the pressure distributions on the flat plate compared with the measured ones along the constant y lines. The agreement is good although the computation generally overpredicts especially near the maximum thickness of the strut (x=0.18). This trend is similar to Sung's computation[19]. Sung claimed that one possible source for this discrepancy is the blockage effect of the wind tunnel. However more careful examination seems to be necessary because Burke's one[12] shows also overpredicted pressure distribution although he includes the wind tunnel wall in his computation.

Figs.9 to 13 compare the cross flow velocity vectors and longitudinal velocity contours with the experimental data on the planes at x=0.18, 0.75, 0.93, 1.05 and 1.5 which are shown in Fig.3. At x=0.18, where the thickness of the strut is maximum, geometry induced or pressure driven outward cross flows are so dominant that they mask the horseshoe vortices. However, at x=0.75, where the geometry induced flow becomes weak, the primary horseshoe vortex can be detected from

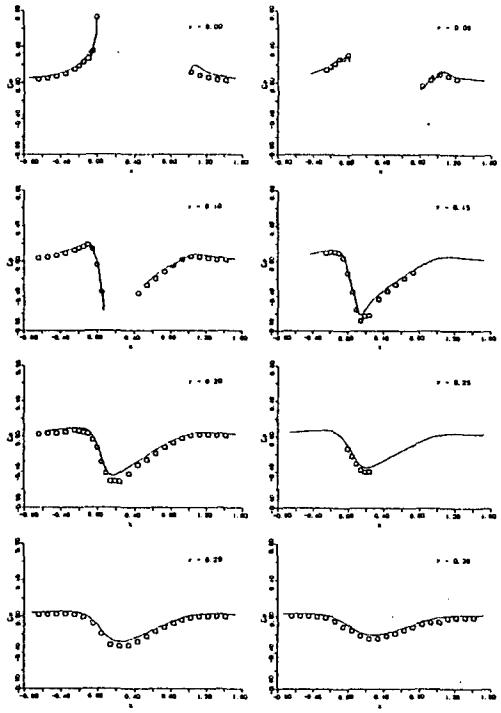

Fig. 8 Pressure distribution on the plate

the decrease of inward velocity, which lies close to the plate around y=0.2. The secondary horseshoe vortex is seen near the corner at x=0.18, which could not be observed in the experimental data due to the insufficient measuring data. The existence of the primary vortex can be seen also from the depressions in the contours of streamwise velocity. These depressions are the result of the momentum transfer by the horseshoe vortex between the slow flow near the plate and the flow with higher momentum away from the plate. These depressions become bigger and wider as flow goes downstream since the size of horseshoe vortex becomes larger due to the diffusion. At x=0.93, just ahead of the trailing edge, computation predicts a separation near the corner but separation does not occur in the experimental data. Further examination for the treatment of the turbulent transport and grid

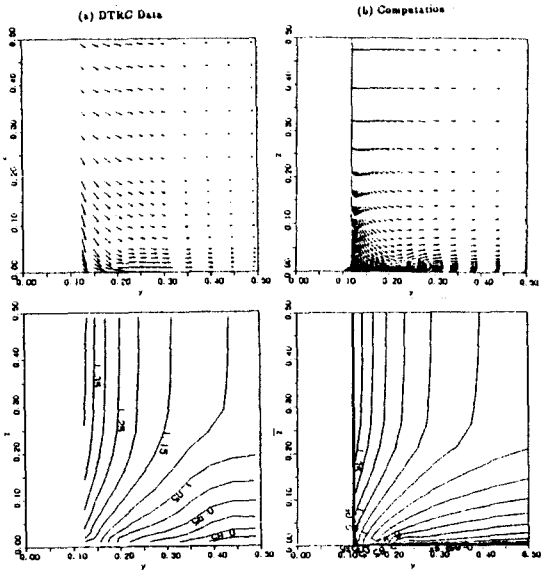

Fig. 9 Comparison of cross-flow velocity vectors and streamwise velocity contours at x=0.18

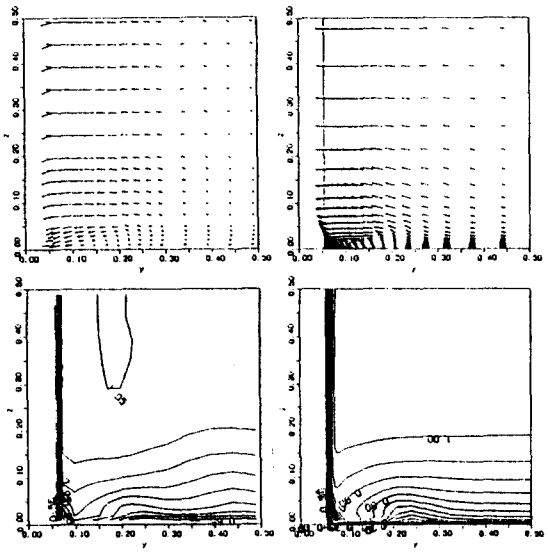

Fig. 10 Comparison of cross-flow velocity vectors and streamwise velocity contours at x=0.75

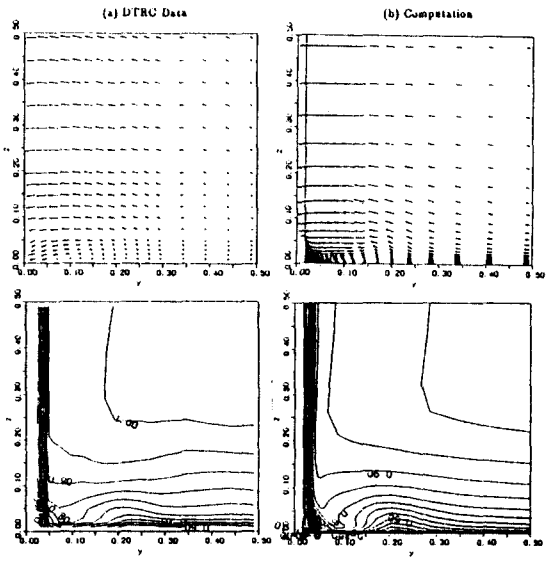

Fig. 11 Comparison of cross-flow velocity vectors and rtreamwise velocity contours at x=0.93

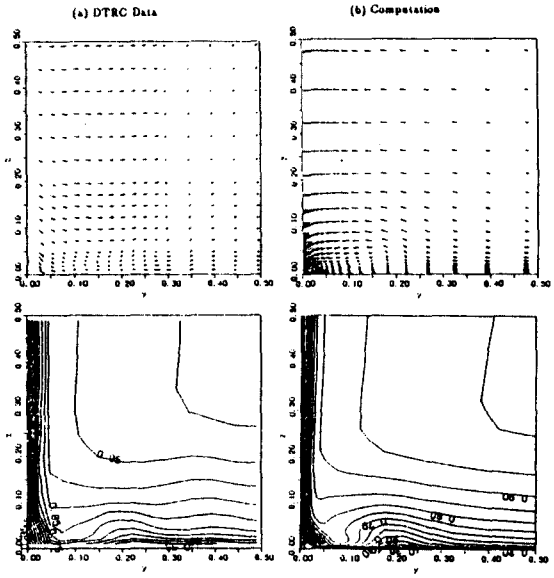

Fig. 12 Comparison of cross-flow velocity vectors and streamwise velocity contours at x=1.05

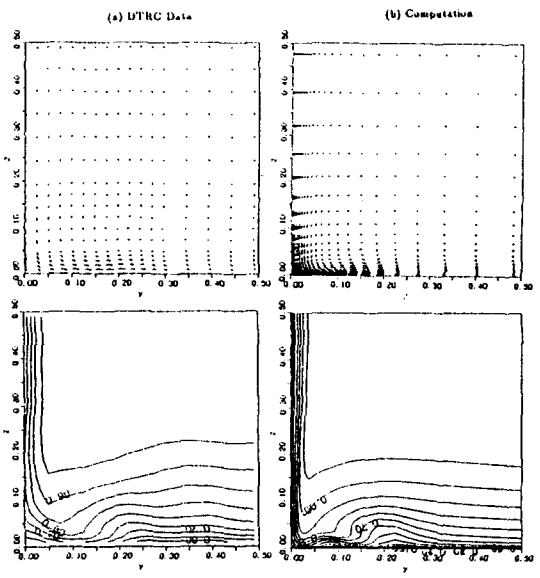

Fig. 13 Comparison of cross-flow velocity vectors and steamwise velocity contours at x=1.5

refinement would be necessary to enlighten the reason for the prediction of earlier separation.

It should be noticed here that Sung[10] and Patel[11] also found the separation in their computed results on this plane; they use the Baldwin-Lomax model and two-layer model as a turbulence model, respectively. Strong trailing edge vortex is observed at x=1.05, just behind the trailing edge, although it is difficult to find out it in the experimental data. The outward velocity at x=1.05 in the experimental data seems to be erroneous as Sung[10] discussed. At x=1.5, in the far wake, the pressure driven cross flow velocity almost disappears and the vortex can be clearly seen. The computation predicts the vortex very well but the core of the vortex is a little lower and closer to the symmetry plane compared with the experimental data.

A more detailed comparison of the velocity profiles normal to the plate and normal to the strut are given in Fig.14 and Fig.15. Generally they show good agreements except near the region very close to the juncture. Computation

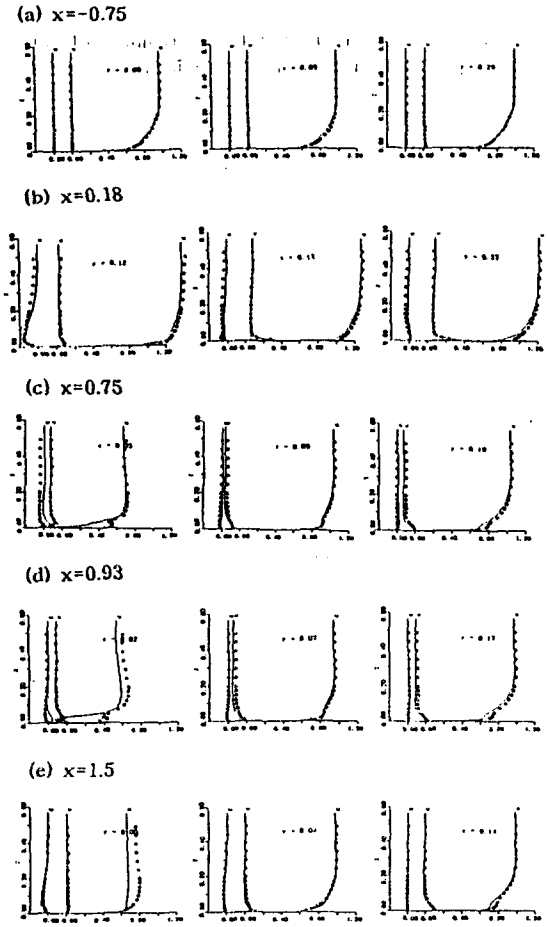

Fig. 14 Comparison of velocity profiles normal to the plate(∘ ∘ ∘ : measured, —— : computed)

underpredicts u, the streamwise component of velocity, near the juncture. The deviation becomes larger as the flow goes to the trailing edge and the computation predicts the earlier separation at x=0.75. However the influence of the separation is confined to the juncture region and the profiles agree well outside the juncture. Relatively, the cross flow velocity component v, w are simulated well so that we can say that the horseshoe vortex is properly captured in the computation. In the wake, the computed wake is much smaller than the measured one on the symmetric plane all over the height although the comparison shows

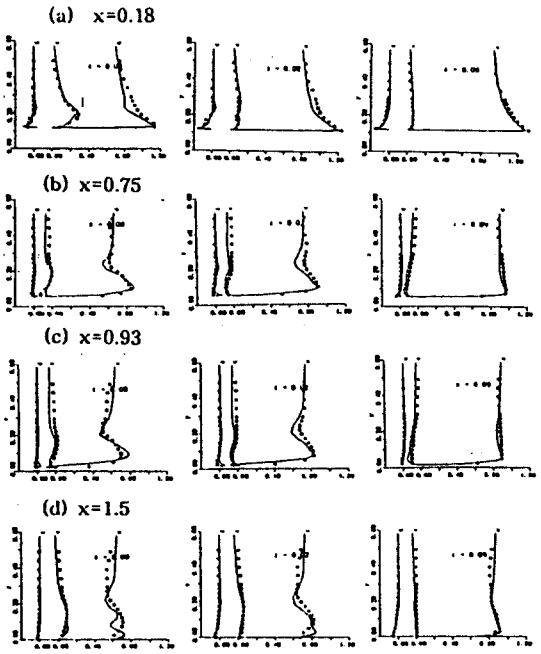

Fig. 15 Comparison of velocity profiles normal to the strut(∘ ∘ ∘ : measured, —— : computed)

good agreements in the region a little apart from the symmetry plane. Increasing the grids in the wake can not improve the prediction so much because the prediction of smaller wake is observed only on the symmetry plane. Some special treatment of the computation on the symmetry plane seems to be required.

Fig.16 and Fig.17 show the comparison of the Reynolds stress profiles $-\overline{uv}$ and $-\overline{uw}$.

The computed Reynolds stress follow the measured data qualitatively. However, they show large differences in the wake even qualitatively. The measured Reynolds stresses are large on the symmetry plane but computed ones are zero because of symmetry condition. In addition, the computed and measured Reynolds stress $-\overline{uv}$ shows opposite sign near the symmetry plane. These mean that the Reynolds stress are not in proportion to the velocity gradient in the wake of the juncture flow. In other words, the eddy viscosity

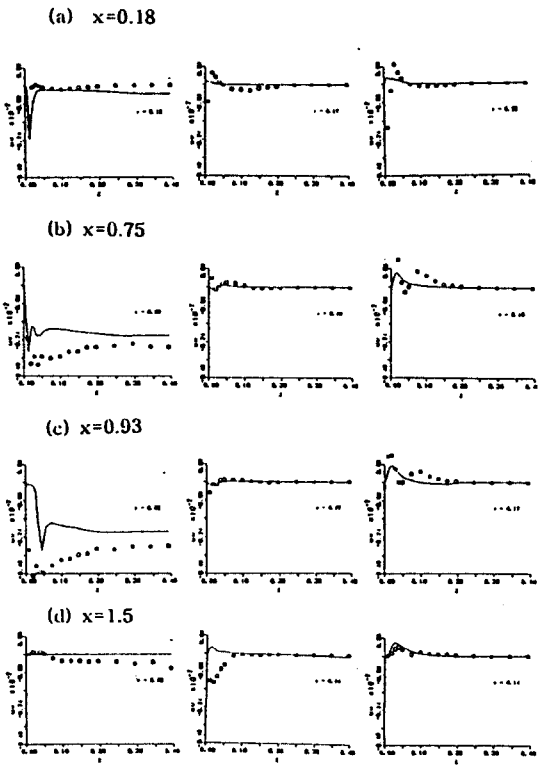

Fig. 16 Comparison of $\overline{uv}$ reynoldsstress profiles (∘ ∘ ∘ : measured, —— : computed)

model itself is not valid in this region. The same argument can be made with measured velocities and Reynolds stresses since the computed and measured velocities have same sign at least. The similar discussions can be found also in many other experimental studies[20-23]. To predict the flow more accurately in the wake of juncture flow, the more advanced turbulence model seems to be required. The algebraic stress model, one of second closure turbulence model, may be promising one.

4. Conclusion

The computational method for the turbulent juncture flow is presented in this paper. Computations are made by solving

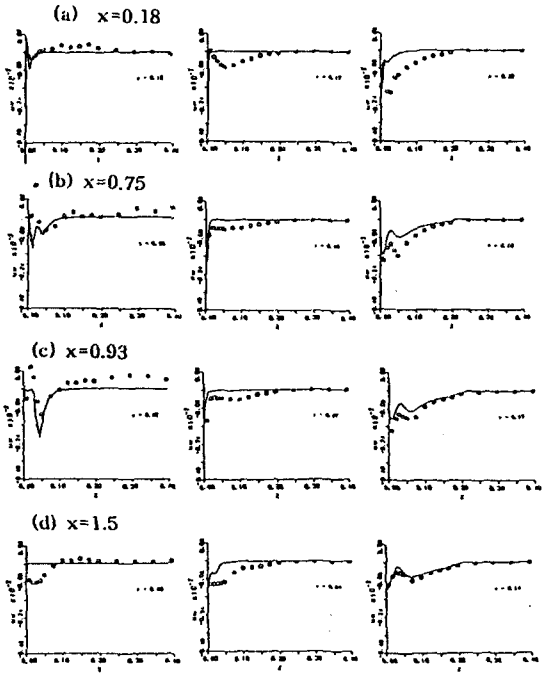

Fig. 17 Comparison of $\overline{uw}$ Reynolds stress profiles (∘ ∘ ∘: measured, —— : computed)

Reynolds-averaged Navier-Stokes equation with MAC method and the turbulence transport is modelled with a Baldwin-Lomax model and Buleev's modified length scale.

To validate the computational method, the computed results are compared with experimental data. The comparisons show good agreements generally. The introduction of the modified length and Baldwin-Lomax model seems to give a reasonable prediction even for the complicated juncture flow. However, some discrepancies are observed very near the juncture and in the wake. The more study for the treatment of Baldwin-Lomax model in this region seems to be required. Since the eddy-viscosity assumption is not valid in the wake, introduction of the algebraic stress model to the juncture flow would be an interesting topic for the future research.

References

[1] Kim, S. Y. and Mori, K., "A Study on the Flow around a Strut Mounted on a Plate with an Angle of Attack", *J. of Society of Naval Architects of Japan*, Vol. 171, pp. 13-25, 1992.

[2] Kim, S. Y. and Mori, K., "A Study on Juncture Flows; Effects of the Inclination of Strut and the Curvature of Plate", *J. of Society of Naval Architects of Japan*, Vol. 172, pp. 267-275, 1992.

[3] Dickinson S. C., "An Experimental Investigation of Appendage-Flat Plate Junction Flow", *DTNSRDC Report DTNSRDC-86/052*, 1986.

[4] Baker, C. J., "The Laminar Horseshoe Vortex", *J. of Fluid Mechanics*, Vol. 95, pp. 347-367, 1979.

[5] Devenport, W. J. and Simpson, R. L., "The Turbulence Flow Structure Near an Appendage-Body Junction", *17th Symposium on Naval Hydrodynamics*, pp. 461-473, 1988.

[6] Devenport, W. J. and Simpson, R. L., "The Flow Past a Wing-Body Junction - An Experimental Evaluation of Turbulence Models", *18th Symposium on Naval Hydrodynamics*, pp. 39-52, 1990.

[7] Menna, J. D. and Pierce, F. J., "The Mean Flow Structure Around and Within a Turbulent Junction or Horseshoe Vortex -Part1 : The Upstream and Surrounding Three-Dimensional Boundary Layer", *J. of Fluid Engineering*, Vol. 110, pp. 406-414, 1988.

[8] Pierce, F. J. and Harsh, M. D., "The Mean Flow Structure Around and Within a Turbulent Junction or Horseshoe Vortex -Part2 : The Separated and Junction Vortex Flow", *J. of Fluid Engineering*, Vol. 110, pp. 415-423, 1988.

[9] Angui, J. and Andreopoulos, J., "Experimental Investigation of a Three-Dimensional Boundary Layer Flow

in the Vicinity of an Upright Wall Mounted Cylinder", *J. of Fluid Engineering*, Vol. 114, pp. 566-573, 1992

[10] Sung, C. H. and Yang, C. -I., "Validation of Turbulent Horseshoe Vortex Flows", *17th Symposium on Naval Hydrodynamics*, pp. 566-576, 1988.

[11] Chen, H. C. and Patel, V. C., "The Flow Around Wing-Body Junctions", *Proc. 4th Num. Physical Aspects Aerodynamic Flows*, pp. 241-255, 1989.

[12] Burke, R. W., "Computation of Turbulent Incompressible Wing-Body Junction Flow", *AIAA Paper* 89-0279, 1989.

[13] Baldwin, B. S. and Lomax, H., "Thin-Layer Approximation and Algebraic Model for Separated Turbulent Flows", *AIAA Paper* 78-257, 1978.

[14] Hung, C. M. and Buning, P. G., "Simulatio n of Blunt-Fin Induced Shock-Wave and Turbulent Boundary-Layer Interaction", *J. of Fluid Mechanics*, Vol. 154, pp. 163-185, 1985.

[15] Buleev, N. I., "Theoretical Model of the Mechanism of Turbulent Exchange in Fluid Flow", *AERE Translation* 957, 1963.

[16] Visbal, M. R. and Knight, D., "The Baldwin-Lomax Turbulence Model for Two-Dimensional Shock-Wave /Boundary -Layer Interactions", *AIAA J.*, Vol. 22, N o. 7, pp. 921-928, 1984.

[17] Mori, K. and Kim, S. Y. and "A Study on the Flow Structure around a Strut Mounted on a Plate", *Hull Form 92': Workshop on Hull Form Design and Flow Phenomena*, at Inha Univ., 1992.

[18] Kim, S. Y. "A Study on the Flow around a Strut Mounted on a Plate", Ph.D. Thesis Hiroshima University, 1993.

[19] Sung, C. H., "An Implicit Runge-Kutta Method for 3D Turbulent Incompressible Flows", *DTNSRDC, Report DTNSRDC/ SHD*-1244-01, 1987.

[20] Shabaka, I.M.M.A. and Bradshaw, P., "Turbulent Flow Measurements in an Idealized Wing/Body Junction", *AIAA J.*, Vol. 19, No. 2, pp. 131-132, 1981.

[21] Nakamaya, A and Rahai, H. R., "Measurements of Turbulent Flow Behind a Flat Plate Mounted Normal to the Wall", *AIAA J.*, Vol. 22, No. 12, pp. 1817-1819, 1984.

[22] Chang, P. S. and Gessner, F. B., "Experimental Investigation of Flow About a Strut-Endwall Configuration", *AIAA J.*, Vol. 29, No. 12, pp. 2105-2114, 1991.

[23] Merati, P., McMahon, H. M. and Yoo, K. M., "Experimental Investigation of a Turbulent Flow in the Vicinity of an Appendage Mounted on a Flat Plate", *J. of Fluids Engineering*, Vol. 113, pp. 635-642, 1991.